

Inverse-square law between time and amplitude for crossing tipping thresholds

Paul Ritchie*

*Earth System Science, College of Life and Environmental Sciences,
Harrison Building, University of Exeter, Exeter, EX4 4QF, United Kingdom*

Özkan Karabacak†

*Centre for Systems, Dynamics and Control, College of Engineering,
Mathematics and Physical Sciences, Harrison Building,
University of Exeter, Exeter, EX4 4QF, United Kingdom and
Department of Electronics and Communication Engineering,
Istanbul Technical University, 34469 Istanbul, Turkey*

Jan Sieber‡

*Centre for Systems, Dynamics and Control, College of Engineering,
Mathematics and Physical Sciences, Harrison Building,
University of Exeter, Exeter, EX4 4QF, United Kingdom*

(Dated: December 14, 2024)

A classical scenario for tipping is that a dynamical system experiences a slow parameter drift across a fold (usually caused by a run-away positive feedback loop). We study how rapidly one needs to turn around once one has crossed the threshold. We derive a simple criterion that relates the peak and curvature of the parameter path in an inverse-square law to easily observable properties of the dynamical system near the fold.

For the case when the dynamical system is subject to stochastic forcing we give an approximation to the probability of tipping for parameter paths that are turning around near the tipping point.

We apply these approximations to investigate when dynamic changes of the albedo across a critical value cause tipping in a model for the Indian Summer Monsoon. The model, originally derived by Zickfeld *et al.*, describes the positive moisture advection feedback between the Indian Ocean and the Indian subcontinent using two dynamic variables, the atmospheric temperature and specific humidity over land. The inverse-square law between time spent at elevated albedos and amplitude of increase beyond the tipping threshold is visible in the level curves of equal probability when the system is subject to random disturbances.

A common scenario in nonlinear systems is that they possess thresholds in parameter space (so-called bifurcations) where their steady-state behaviour changes qualitatively. For example, in simple models of the Indian Summer Monsoon, increasing the planetary albedo A (reflection of incoming sun-light due to whiteness of the surface), causes the Summer Monsoon to shut down. The underlying mechanism is a run-away positive feedback effect between moisture advection and the temperature difference between the land and ocean. In the mathematical model this effect creates a fold of steady states: a stable steady state of the system disappears at some critical value of the albedo A^b (the *tipping point*) in a fold (becoming unstable).

When the albedo A changes over time, increasing beyond the tipping threshold A^b , the monsoon will shut down. This shutdown is slightly delayed compared to the crossing, if

the change of albedo is relatively fast, giving time to avoid tipping when the albedo change is reversed. The relation between the time t which the albedo may spend above the level A^b and the maximal amount $q = \max_t(A(t)) - A^b$ by which the albedo may exceed the level A^b follows an inverse-square law: if $q \times t^2$ is less than a critical level $16/d$ then tipping is avoided, when it is larger than $16/d$, tipping occurs. The level d is the derivative with respect to the parameter of the square of the decay rate toward stable equilibria near the fold. The quantity d can thus be estimated from the autocorrelation in time series of system outputs. The inverse-square relation holds approximately for all cases of tipping caused by positive feedback (folds).

If the system is subject to random disturbances the level curves of equal probability (for example, the set of exceedance times t and exceedance amplitudes q where tipping probability is 50%) also follow similar inverse-square laws approximately. We provide a few general approximation formulas for these probabilities and test them on the In-

* Paul.Ritchie@exeter.ac.uk

† O.Karabacak@exeter.ac.uk

‡ J.Sieber@exeter.ac.uk

dian Summer Monsoon model.

I. INTRODUCTION

The phenomenon of tipping is subject to ongoing intense study within the scientific community due to its prominence in complex systems, including climate [1–4], ecosystems [5, 6] and finance [7]. The notion of tipping usually refers to a sudden large qualitative change in output behaviour caused by a small change to input levels or rates [8]. The classical and most common model case for tipping is that the system can be described (possibly at a coarse level) as a dynamical system with a slowly drifting system parameter which passes slowly through a fold (or saddle-node) bifurcation. In scientific terms the mathematical scenario of a fold bifurcation at some system parameter value corresponds to the presence of internal positive feedback loops, which, with sufficient internal amplification, lead to a run-away scenario.

In Section III we will introduce a simple Indian Summer Monsoon model, originally derived by Zickfeld [9], which we will use for illustration throughout. In this model a positive feedback loop is formed between the temperature difference over the Indian Ocean and Indian subcontinent and moisture advection [10]. In the summer months the temperature over land warms quicker than the temperature over the ocean, which creates winds coming off the ocean onto land [9]. The winds carry moisture which is deposited over the land in the form of precipitation. This process releases latent heat, causing the temperature over land to increase, creating a greater temperature difference and thus generating stronger winds to complete the positive feedback loop. Zickfeld *et al.* [11] identified a tipping threshold in the planetary albedo, such that increasing the albedo above this value will cause the monsoon to shutdown.

The classical tipping scenario considers a gradual parameter change that varies the system parameter slowly through the tipping threshold (the fold bifurcation parameter value), causing a transition from the current gradually varying equilibrium to a new state, possibly far away in state space. However, we may expect that this transition is delayed with respect to the passage through the tipping threshold if the system is forced at a faster than infinitesimal speed. This delay may pose interesting questions for policy. For example, if we notice that a system has just passed a tipping threshold, how rapidly does one have to reverse the forcing to prevent tipping? We will investigate this for the example model of the Indian Summer Monsoon, one of the policy relevant tipping elements in the climate system identified by Lenton *et al.* [1]. For this climate subsystem, policy makers may be interested in understanding: if the albedo was increased past the threshold, can the albedo be reversed quickly enough to prevent a shutdown of the monsoon? We show that for Zickfeld’s model the maximal permitted exceedance value and time over the tipping threshold follow an in-

verse square law.

General deterministic result (see Section II) Let us assume without loss of generality that the system has a fold in system parameter q at value q^b , that the stable equilibrium exists for $q < q^b$, that the parameter path $q(t)$ is approximately parabolic near the tipping point, reaching a maximum value $q_{\max} > q^b$, and that the non-linearity of the system near the tipping point is dominated by quadratic terms (as is the case near fold bifurcations). Then the inverse square law contains only one system specific proportionality factor d , which is independent of the path parameters. More precisely, tipping is avoided when following the parameter path $q(t)$ if

$$\underbrace{\left[\frac{\partial}{\partial q} [(-\lambda(q))^2] \Big|_{q=q^b} \right]}_d (q_{\max} - q^b) t_e^2 \leq 16.$$

In this expression $\lambda(q)$ is the leading eigenvalue of the linearization of the system in the stable equilibrium. In real-world applications there is often no direct access to an underlying model. Instead, only time series output data, disturbed by random fluctuations, may be available, such as proxies for the temperature and CO_2 [12] in palaeo-climate records. One may estimate the quantity d from the autocorrelation $a(q)$ of a times series with approximately stationary parameter q close to the critical value q^b via

$$d \approx \frac{(1 - a(q))^2}{q - q^b} \quad \text{for } q < q^b, q \approx q^b.$$

The autocorrelation and variance of output time series are expected to increase in the case that the parameter path $q(t)$ crosses the critical value q^b sufficiently slowly. This has motivated extensive studies in field data (such as palaeo climate records or lake sediments), investigating whether autocorrelation and variance act as *early-warning indicators* of tipping [13–16]. See also Ritchie and Sieber [17] for a study on the behaviour of early-warning indicators when the parameter is changed at higher speed, causing rate-induced tipping.

Probabilistic result (see Section IV) If the system is subject to random disturbances, tipping may occur with positive probability even if the parameter path $q(t)$ never exceeds q^b . Thus, the exceedance time $t_e(q_0)$ for arbitrary fixed parameter values $q_0 < q^b$ (but close to q^b) becomes a relevant parameter ($t_e(q_0)$ is the time which the path spends above level q_0).

In these parameters we find that the level curves of constant probability of tipping follow the inverse square law approximately in parts of the $((q_{\max} - q^b)D^{-2/3}, t_e(q_0)D^{1/3})$ two-parameter plane. Here $2D$ is the variance of the random forcing (assumed to be white noise), projected onto the critical direction. We provide a numerically computed graph of escape probabilities that is accurate in the limit of slow parabolic paths and small noise. We also provide approximations for the

escape probabilities in several limiting cases of the provided graph.

In Section V we will illustrate the escape probability estimates for the monsoon model with additive noise. After the summary in Section VI, appendices will give detailed expressions for the projection of the n -dimensional system onto a scalar ODE, and for the approximations of the escape probability in the presence of noise.

II. CRITICAL DISTANCE AND TIME OVER THRESHOLD BEFORE TIPPING

We consider an n -dimensional system of ordinary differential equations (ODEs)

$$\dot{\mathbf{y}} = f(\mathbf{y}, q), \quad \mathbf{y} \in \mathbb{R}^n, q \in \mathbb{R} \quad (1)$$

that has a fold (saddle-node) bifurcation at $(\mathbf{y}, q) = (\mathbf{y}^b, q^b)$ when one varies q as a (time-independent) parameter. This section will study the question how this bifurcation changes when the parameter q drifts slowly in time along a path $q(t)$. We do not assume that the parameter q passes through its bifurcation value q^b transversally (which is usually the case when $\lim_{t \rightarrow -\infty} q(t) < q^b$ and $\lim_{t \rightarrow \infty} q(t) > q^b$), but rather focus on the case where the path

- (A1) starts at q^∞ on the side of the fold with a stable equilibrium for $t \rightarrow -\infty$ (we assume that $q^\infty < q^b$ without loss of generality),
- (A2) “peeks across the bifurcation value q^b briefly” at its maximum $q^\infty + r > q^b$ at $t = 0$,
- (A3) and then returns to the parameter regime with a stable equilibrium, converging exponentially back to q^∞ for $t \rightarrow +\infty$.

See Figure 1a for a typical shape of $q(t)$ for our illustrative example of the Indian Summer Monsoon model. If we assume exponential convergence of $q(t)$ to q^∞ for $t \rightarrow \pm\infty$, strict monotone growth for $t < 0$ and strict monotone decay for $t > 0$, we can describe q with a differential equation:

$$q(t) = q^\infty + r\Gamma(\mu(t)) \quad \text{where} \quad \dot{\mu} = \epsilon\Gamma'(\mu). \quad (2)$$

For a given path $q(t)$, the scalar parameters $r > 0$ and $\epsilon > 0$, and the functions $\mu : \mathbb{R} \mapsto [0, 1]$ and $\Gamma : [0, 1] \mapsto [0, 1]$ are

$$\begin{aligned} r &:= \max_t q(t) - \lim_{t \rightarrow \pm\infty} q(t) = q(0) - q^\infty, \\ \epsilon &:= \left[\int_{-\infty}^{\infty} \frac{q(s) - q^\infty}{q(0) - q^\infty} ds \right]^{-1} = \left[\int_{-\infty}^{\infty} \frac{q(s) - q^\infty}{r} ds \right]^{-1}, \\ \mu(t) &:= \frac{\epsilon}{r} \int_{-\infty}^t q(s) - q^\infty ds, \quad \Gamma(\mu) := \frac{1}{r} [q(\tau(\mu)) - q^\infty]. \end{aligned}$$

In the definition of Γ we exploited that μ is monotone such that $t \mapsto \mu$ is invertible, calling its inverse $\tau : (0, 1) \mapsto \mathbb{R}$. The function $q(\tau(\mu))$ has a well-behaved

limit for $\mu \rightarrow 0$ and $\mu \rightarrow 1$, as we assume that q is monotone for large $|t|$ and converges exponentially to q^∞ for $t \rightarrow \pm\infty$. Thus, notation (2) introduces four parameters to describe the parameter path:

- q^∞ : its asymptotic value,
- r : its maximum excursion (distance from q^∞),
- ϵ : the inverse of the area under $(q(t) - q^\infty)/r$,
- Γ : a normalized function describing other aspects of the path.

The function $\Gamma(\mu)$ satisfies the following properties:

$$0 = \Gamma(0) = \Gamma(1),$$

$$1 = \Gamma(\mu_c) = \max\{\Gamma(\mu) : \mu \in [0, 1]\}, \text{ this defines } \mu_c = \mu(0)$$

$$0 > \Gamma''(\mu_c)$$

$$\Gamma(\mu) \in (0, 1) \text{ for all } \mu \in (0, \mu_c) \text{ and } \mu \in (\mu_c, 1).$$

Throughout our paper we assume that the parameter ϵ is small, making the system with drift, (1)–(2), a slow-fast autonomous system with a $n+1$ -dimensional phase space. Smallness of the parameter ϵ automatically implies that higher-order time derivatives of q will be small:

$$\begin{aligned} \frac{d^k}{dt^k} q(t) &\sim \epsilon^k \quad \text{for } k \geq 1, \text{ in particular,} \\ \left. \frac{d^2}{dt^2} q(t) \right|_{t=0} &= \epsilon^2 r \Gamma''(\mu(0)). \end{aligned} \quad (3)$$

Thus, when we expand the path $q(t)$ with respect to time we are justified in dropping higher-order time derivatives of the path. Note that, although we assume that q can be described by (2), our analysis requires only the smallness condition (3) on its derivatives.

We assume that we have for fixed $q \in [q^\infty, q^b)$ a branch of stable equilibria (\mathbf{y}_q^s, q) and a branch of unstable equilibria (\mathbf{y}_q^u, q) of (1) (all satisfying $0 = f(\mathbf{y}_q^{s,u}, q)$), which meet in the fold at (\mathbf{y}^b, q^b) . We expect the solution $(\mathbf{y}(t), \mu(t))$, starting from $(\mathbf{y}_{q^\infty}^s, 0)$ to follow the stable branch closely for sufficiently small ϵ until we reach the vicinity of (\mathbf{y}^b, q^b) , at time t close to 0.

Assume that we observe a scalar output $y_o(t) = \mathbf{w}^T \mathbf{y}(t)$. In the vicinity of the fold bifurcation (\mathbf{y}^b, q^b) , we may zoom in and speed up time:

$$\begin{aligned} x &:= \epsilon^{-1/2} (y_o - y_o^b) = \epsilon^{-1/2} \mathbf{w}^T (\mathbf{y} - \mathbf{y}^b), \\ R_0 &:= \epsilon^{-1} (r - q^b + q^\infty), \quad R_2 := \frac{q^\infty - q^b}{2} \Gamma''(\mu_c) \quad (4) \\ t_{\text{new}} &:= \epsilon^{1/2} t_{\text{old}}. \end{aligned}$$

Then, generically, x satisfies a scalar differential equation of the form.

$$\dot{x} = a_0 (R_0 - R_2 t^2 + \kappa x^2) + O(\epsilon^{1/2}). \quad (5)$$

It is clear that, if $r - q^b \gg \epsilon$ (thus, $R_0 \gg 1$), the trajectory $y(t)$ will leave the neighborhood of the branches of equilibria (corresponding to tipping). Thus, only paths $q(t)$ with $q(0) = r + q^\infty = q^b + O(\epsilon)$ (that is, R_0 of order 1) are of interest.

The quantities a_0 and κ can be estimated from observations of the output x for fixed parameter ($\epsilon = 0$, thus, $R_2 = 0$): 2κ is the curvature of the equilibrium curve as observed through x in $x = 0$, and the decay rate for parameter values equal to R_0 (for $R_2 = 0$) toward the stable equilibrium for $R_0\kappa < 0$ equals $-2a_0\sqrt{-R_0\kappa}$. Note that this is the decay rate for the zoomed in x . See Appendix A for expressions of a_0 and κ depending on f and for the required genericity conditions.

To fix notation we assume that the sign of the output x is chosen such that $\kappa > 0$, and that $a_0 > 0$ (that is, $q^b > q^\infty$). In the limit $\epsilon = 0$, the scalar equation (5) has solutions that are asymptotically $x(t) \sim -|t|\sqrt{R_2/\kappa}$ for large t if

$$R_0 < \frac{1}{a_0} \sqrt{\frac{R_2}{\kappa}}. \quad (6)$$

The limiting orbit of (5), for $\kappa a_0^2 R_0^2 = R_2$ and $\epsilon = 0$, is $x(t) = t\sqrt{R_2/\kappa}$. In the original coordinates, this gives a first-order expansion for the critical value r_{crit} of r , the amount by which the path $q(t)$ may exceed q^∞ without causing tipping:

$$r_{\text{crit}}(\epsilon, \Gamma) = q^b - q^\infty + \frac{\epsilon}{a_0} \sqrt{\left. \frac{q^\infty - q^b}{2\kappa} \frac{d^2\Gamma}{d\mu^2} \right|_{\mu=\mu_c}} + o(\epsilon). \quad (7)$$

Alternatively, in terms of the original path $q(t)$, this expansion may be expressed as a condition relating the maximum value of q (which it attains at $t = 0$: $q(0) = \max_t q(t)$) and its second derivative $\ddot{q}(0)$ at $t = 0$ to each other. The system does not experience tipping if

$$q(0) - q^b < \frac{1}{a_0} \sqrt{-\frac{\ddot{q}(0)}{2\kappa}} + O(\epsilon). \quad (8)$$

The combination of the bifurcation quantities a_0 and κ , needed for (8), $1/(a_0\sqrt{2\kappa})$, may be found via the quantity

$$d := \frac{\partial}{\partial q} [(-\lambda(q))^2] \Big|_{q=q^b} = \lim_{q \rightarrow q^b} \frac{[-\lambda(q)]^2}{q^b - q}, \quad (9)$$

where $\lambda(q)$ is the leading eigenvalue of the linearization of underlying system (1) toward the stable equilibrium y_q^s (or, equivalently, the decay rate toward y_q^s) in the original time-scale t_{old} and spatial scale \mathbf{y} . Then $d = 4a_0^2\kappa$, such that

$$q(0) - q^b < \sqrt{-\frac{2\ddot{q}(0)}{d}}, \quad (10)$$

where both, d and $\ddot{q}(0)$, are computed in the original scaling for parameter, space and time. Thus, to establish the critical permissible distance $\max_t q(t) - q^b$ over the threshold before tipping, we need some estimate of the attraction rate toward the stable equilibria near the fold. This decay rate can, for example, be estimated through the autocorrelation in the output time series $x(t)$ when the system is subject to fluctuations

[12–14, 18]. The inequalities (8) and (10) assume that the higher-order derivatives of q are small compared to its second derivative near its maximum. If q is given by a differential equation then the smallness of ϵ ensures the smallness of these higher-order derivatives. At the critical value r_{crit} , given in (7) the extended autonomous system (where the path q is given by a differential equation for μ) has a connecting orbit from the equilibrium $E_{-\infty} = (\mathbf{y}_{-\infty}, \mu_{-\infty}) = (y_{q^\infty}^s, 0)$ to the equilibrium $E_\infty = (\mathbf{y}_\infty, \mu_\infty) = (y_{q^\infty}^u, 1)$. Both equilibria are saddle equilibria of the extended system (1)–(2): $E_{-\infty}$ is unstable in its last component μ , E_∞ has at least one unstable direction in its \mathbf{y} component and is stable in the μ direction.

Furthermore, for every $R_0 > 0$ (or $r > q^b$) and given Γ (or given $q(t)$) we can introduce an alternative parameter to $\ddot{q}(0)$: let the exceedance time t_e be the time that the parameter path $q(t)$ spends beyond the fold bifurcation value q^b . In the original time-scale, the relationship between t_e and the other system parameters is approximately

$$\begin{aligned} t_e &= \sqrt{\frac{8(q^b - q(0))}{\ddot{q}(0)}} + O(1) \\ &= \epsilon^{-1/2} \sqrt{\frac{8R_0}{(q^\infty - q^b)\Gamma''(\mu_c)}} + O(1). \end{aligned} \quad (11)$$

As the second expression (using the parametrization of q with the slow differential equation (2) for μ) makes clear, this critical exceedance time t_e is large (of order $\epsilon^{-1/2}$), even when the amplitude of the exceedance ϵR_0 is small (R_0 is of order 1 as it is the rescaled maximum r of the excursion of the path q). We can then insert relation (11) into (10) to establish the inverse-square law for maximal exceedance $q(0) - q^b$ and time of exceedance t_e that avoids tipping (recall that $q(0) = \max_t q(t)$ and d is given by (9)):

$$d [q(0) - q^b] t_e^2 \leq 16, \quad \text{or,} \quad a_0^2 \kappa [q(0) - q^b] t_e^2 \leq 4. \quad (12)$$

The above inequality is a valid criterion for the tipping threshold if $q(0) - q^b$ is small in modulus (of order ϵ), while t_e is large. The inequality assumes also that higher order derivatives of the path $q(t)$ are small. It becomes a sharp criterion asymptotically in the limit $\epsilon \rightarrow 0$.

In the following section we will test the approximation (12) on a model for the Indian Summer Monsoon which displays tipping (shutting ‘off’ the monsoon) for increasing planetary albedo.

III. INDIAN SUMMER MONSOON MODEL

We consider a model for one of the recognised policy-relevant tipping elements in the Climate System, the Indian Summer Monsoon [1]. The key driving force of the monsoon is the moisture-advection feedback loop [10]. In

the summer months the land is warmer than the ocean. This temperature difference generates winds coming off the Indian ocean onto the land. The winds carry moisture from the ocean which is deposited over the land in the form of precipitation. This process releases latent heat, meaning that the temperature over land increases. A larger temperature difference causes stronger winds carrying more moisture and hence the positive feedback loop is formed.

We use a model proposed by Zickfeld [9] and make further simplifications, though retaining the key mechanism of the monsoon, the positive feedback loop described above. Two components, the specific humidity q_a and the atmospheric temperature T_a , are described by the following ODEs:

$$\dot{q}_a = \frac{E - P + A_v}{\beta I_q}, \quad (13)$$

$$\dot{T}_a = \frac{\mathcal{L}(P - E) - F_{\uparrow}^{LW,TA} + F_{\downarrow}^{SL,TA}(1 - A_{sys}) + A_T}{\beta I_T} \quad (14)$$

where the terms on the right-hand side are grouped as follows:

- Evaporation E (mm/s): Proportional to the temperature difference between the land T_a and the Indian Ocean T_{oc} and to the difference between saturated humidity q_{sat} and specific humidity q_a

$$E := E(q_a, T_a) = C_E(T_a - T_{oc})(q_{sat} - q_a).$$

- Precipitation P (mm/s): Proportional to the specific humidity

$$P := P(q_a) = C_P q_a.$$

- Moisture advection A_v (mm/s): Winds driven by the temperature difference between the land and ocean bring moisture from the ocean over land proportional to the humidity over the ocean q_{oc} . Winds are reversed above a given height taking moisture away proportional to the humidity over land q_a

$$A_v := A_v(q_a, T_a) = (T_a - T_{oc})(C_{mo}q_{oc} - C_{ml}q_a).$$

- Outgoing long-wave radiation $F_{\uparrow}^{LW,TA}$ (kg/s³): Proportional to the temperature of the land

$$F_{\uparrow}^{LW,TA} := F_{\uparrow}^{LW,TA}(T_a) = C_{L1}T_a + C_{L2}.$$

- Incoming short-wave radiation $F_{\downarrow}^{SL,TA}$ (kg/s³): Fraction of incoming solar radiation not reflected, proportional to $1 - A_{sys}$, where A_{sys} is the system planetary albedo.

- Heat advection A_T (kg/s³): Winds driven by the temperature difference between the land and ocean bring cool air at a prescribed low altitude proportional to the potential temperature θ_{oc} above

the ocean (θ_{oc} is fixed). Reversed winds at a prescribed high altitude z_h take warm air away proportional to the potential temperature above the land $\theta_a(q_a, T_a)$. The potential temperature at the prescribed height z_h is given by $\theta_a = T_a - (\Gamma(T_a, q_a) - \Gamma_a)z_h$ where $\Gamma = \Gamma_0 + \Gamma_1(T_a - T_0)(1 - \Gamma_2 q_a^2)$ (with a reference temperature T_0) is the atmospheric lapse rate and Γ_a is the adiabatic lapse rate

$$A_T := A_T(q_a, T_a) = C_H(T_a - T_{oc})(\theta_{oc} - \theta_a(q_a, T_a)).$$

The remaining terms are all constants, in particular, latent heat is given by \mathcal{L} , and β provides a conversion from seconds to decades. Appendix C, Table I lists all parameters and their values and units.

Zickfeld *et al.* [11] identified two quantities that are influenced by human activities or subject to natural variation and affect the stability of the monsoon. Either an increase of the planetary albedo A_{sys} or a decrease in the CO_2 concentration from present day values can potentially lead to a “shutdown” of the Indian monsoon. We will focus our analysis on the possibility of an increase in the planetary albedo.

The planetary albedo represents the ratio of reflected to incoming solar radiation and can be influenced by atmospheric aerosols and land-cover conversion [11]. The present day value of the planetary albedo is $A_{sys}^{\infty} = 0.47$. System (13)–(14) has a fold (saddle-node) bifurcation at $A_{sys}^b \approx 0.53$, see Figure 1b. Slowly increasing the planetary albedo linearly beyond the fold will cause tipping in the monsoon model, a sudden drop in the specific humidity would be observed. Equation (14) highlights how increasing the planetary albedo affects the positive feedback loop outlined above. As the albedo is increased, the change in temperature over land decreases, meaning a smaller temperature difference between the land and ocean and hence weaker winds are formed. Our aim is to study how long the planetary albedo can be kept above the fold bifurcation parameter value A_{sys}^b without causing a tipping of the Indian Summer Monsoon. Therefore we choose to force the planetary albedo as detailed in Section II, namely $A_{sys} = A_{sys}^{\infty} + r\Gamma(\mu(t))$, where we choose $\Gamma(\mu) = 4\mu(1 - \mu)$, such that

$$A_{sys}(t) = A_{sys}^{\infty} + 4r\mu(1 - \mu), \quad \text{and} \quad \dot{\mu} = 4\epsilon\mu(1 - \mu) \quad (15)$$

Equation (15) describes increasing the planetary albedo towards (and possibly beyond) the fold bifurcation before it returns to its present day value. Three time profiles of the planetary albedo forcing (15) are given in Figure 1a for illustration. All three fix $\epsilon = 0.5$, which fixes the area under the scaled path $(A_{sys}(t) - A_{sys}^{\infty})/r$, and vary r , the distance of the maximum of the shift from its present day value. The exceedance of the maximum albedo shift r beyond the fold bifurcation (indicated by the horizontal dashed line) and the rate at which it returns to present day values determine whether tipping occurs. The trajectories for each forcing are superimposed on top of the bifurcation diagram for fixed A_{sys} in Figure 1b.

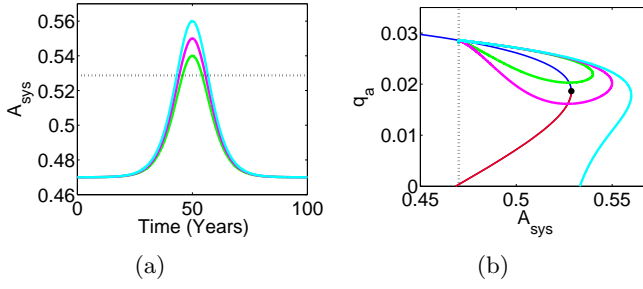


FIG. 1: (a) Time profiles of planetary albedo forcing (15) for $r = 0.07$ (green), $r = 0.08$ (pink) and $r = 0.09$ (bright blue) but fixed $\epsilon = 0.5$, proportional to the time period. Horizontal dotted line indicates location A_{sys}^b of the fold bifurcation. (b) Bifurcation diagram of (13)–(14) in the (A_{sys}, q_a) - plane. Upper branch stable (blue) and lower branch is unstable (red). Superimposed on top are trajectories starting at $A_{\text{sys}}^{\infty} = 0.47$ (vertical dotted line) close to the stable equilibrium branch and subjected to the planetary albedo forcing given in (a).

The green trajectory corresponds to a forcing scenario where the system parameter is increased just beyond the fold before decreasing again. In this scenario the system has little time to escape before the stable branch re-emerges. Increasing A_{sys} further beyond its bifurcation value A_{sys}^b , the trajectory (shown in pink) begins to escape such that when the branches of equilibria reappear the trajectory is initially on the other side of the unstable branch. However, the system recovers fast enough for the trajectory to cross the unstable branch and be attracted back to the stable branch. The final case (bright blue) the planetary albedo is forced sufficiently far beyond the fold bifurcation A_{sys}^b such that the system is unable to recover quickly enough to prevent tipping.

We can calculate numerically the critical curve separating a “safe” area (monsoon retained) from the “unsafe” area, where escape toward shutdown occurs, in the two-parameter plane. We choose as path parameters the peak exceedance beyond the fold $R = \max_t A_{\text{sys}}(t) - A_{\text{sys}}^b$, and exceedance time t_e during which $A_{\text{sys}}(t) > A_{\text{sys}}^b \approx 0.53$.

The critical parameters, for which the exact (numerically computed) connecting orbit to the saddle occurs, are shown as a blue solid curve in Figure 2. As discussed in Section II, the critical amount by which the planetary albedo exceeds the fold value A_{sys}^b is approximately inversely proportional to the square of the time the planetary albedo stays above A_{sys}^b . For example, if the planetary albedo is forced only just above the bifurcation ($R = \max_t A_{\text{sys}}(t) - A_{\text{sys}}^b = 0.005$) then the system can spend a long time (~ 30 years) above the bifurcation value without shutting down the monsoon. However, for a higher maximum of A_{sys} ($R = 0.02$ above the bifurcation value) the system can maintain the monsoon only if the period is shorter (~ 15 years).

The parameter values satisfying the theoretical in-

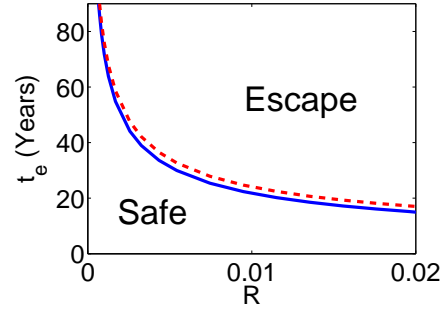


FIG. 2: Tipping region in the two parameter plane $R = \max_t A_{\text{sys}}(t) - A_{\text{sys}}^b$ (Peak distance over fold (saddle-node)) and t_e (Time above fold). Safe region and escape region separated by the numerically calculated critical curve (blue solid). The red dashed curve provides an approximation of the critical curve obtained from equation (12).

equality (12) (valid for the limit $\epsilon \rightarrow 0$) are below the red dashed curve in Figure 2. The curve gives a good approximation to the numerically calculated critical curve. The approximation is best for small critical R_c (peak distance over fold) because then the system spends most time in the region of the phase space where the second-order expansion of the right-hand side in the fold and of the path in its maximum are valid (both of these were assumed in the derivation of inequality (12)).

IV. PROBABILITY OF TIPPING UNDER THE INFLUENCE OF NOISE

In this section we study the probability of tipping when the system is, in addition to its parameter drift, subject to random disturbances, which we model by adding white noise to (1). We again consider a parameter path $q(t)$, which comes close to a fold bifurcation at $t = 0$. We focus on the case where the disturbances are sufficiently small such that escape is unlikely at times when the parameter path $q(t)$ is away from its maximum. Close to the fold the decay rate in the center direction \mathbf{v}_0 is much smaller than the decay rates in the stable directions \mathbf{y}_s , such that disturbances entering through coupling between stable and center directions are small (\mathbf{v}_0 is the right nullvector of $\partial_1 f(\mathbf{y}^b, q^b)$, and $\mathbf{w}_0^T(\mathbf{y}_s - \mathbf{y}^b) = 0$, where \mathbf{w}_0 is the left nullvector of $\partial_1 f(\mathbf{y}^b, q^b)$). If the n -dimensional noise has covariance matrix Δ , its projection onto the scalar output, after the rescaling (4) to the zoomed-in output $x = \epsilon^{1/2} \mathbf{w}^T(\mathbf{y} - \mathbf{y}^b)$ and sped up time, has the variance $\epsilon^{-3/2} \mathbf{w}_0^T \Delta \mathbf{w}_0$, if we scale \mathbf{v}_0 and \mathbf{w}_0 such that $\mathbf{w}^T \mathbf{v}_0 = \mathbf{w}_0^T \mathbf{v}_0 = 1$. Hence, if the variance of the projected additive noise is larger than $O(\epsilon^{3/2})$ the probability of escape will approach 1 for $\epsilon \rightarrow 0$, if the path $q(t)$ comes close to the fold ($\max_t q(t) = q^b + O(\epsilon)$).

Consequently, we assume that the variance of the noise

is of order $\epsilon^{3/2}$ in the original coordinates and focus on the vicinity of the fold, where the rescaled noise variance

$$2D := 2\epsilon^{-3/2} \mathbf{w}_0^T \Delta \mathbf{w}_0$$

is now of order 1. Thus, in the limit for $\epsilon \rightarrow 0$, the projected equation (5) becomes the scalar stochastic differential equation (SDE)

$$dx = a_0[R_0 - R_2 t^2 + \kappa x^2]dt + \sqrt{2D}dW_t \quad (16)$$

(we assume that $a_0 > 0$, $\kappa > 0$ without loss of generality to fix notation). By further rescaling x and time and introducing correspondingly rescaled versions of the parameters R_0 and R_2 ,

$$\begin{aligned} x_{\text{new}} &= \frac{(a_0 \kappa)^{1/3}}{D^{1/3}} x_{\text{old}}, \quad t_{\text{new}} = D^{1/3} (a_0 \kappa)^{2/3} t_{\text{old}}, \\ p_0 &= \frac{a_0^{2/3}}{D^{2/3} \kappa^{1/3}} R_0, \quad p_2 = \frac{R_2}{D^{4/3} \kappa^{5/3} a_0^{2/3}}, \end{aligned} \quad (17)$$

we may simplify (16) to a SDE

$$dx = [p_0 - p_2 t^2 + x^2]dt + \sqrt{2}dW_t \quad (18)$$

with unit noise amplitude and nonlinear coefficient, and the two parameters $p_0 \in \mathbb{R}$ and $p_2 > 0$. The lines

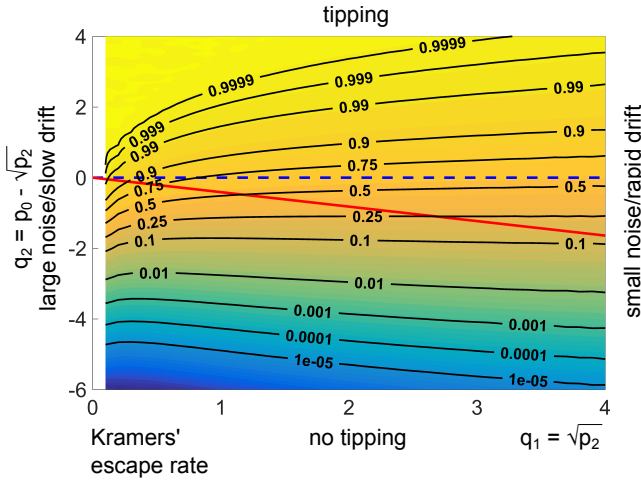


FIG. 3: Probability of escape P_{esc} to $+\infty$ in (18) for intermediate parameter values of $q_1 = \sqrt{p_2}$ and $q_2 = p_0 - \sqrt{p_2}$. Parameters for FPE (19): domain $[-8, 8]$, time interval $[-T_0, T_0]$, initial density $N(x_0, 1)$ where $T_0 = \sqrt{(x_0^2 + p_0)/p_2}$ and $x_0 = -4$.

$x = \sqrt{p_2}t$ for $t \ll -1$ and $x = -\sqrt{p_2}t$ for $t \gg 1$ are stable slow manifolds of the deterministic part of (18). Thus, the density of x at some fixed large time $t = -T_0$ is nearly independent from the initial density for $t \ll -T_0$ (conditional on no escape occurring before $t = -T_0$). Thus, we can compute numerically the probability of escape by solving the Fokker-Planck equation (FPE) for the density $u(x, t)$ of x

$$\partial_t u(x, t) = \partial_x^2 u(x, t) - \partial_x[(p_0 - p_2 t^2 + x^2)u(x, t)] \quad (19)$$

with Dirichlet boundary conditions $u(t, x_{\text{bd}}) = u(t, -x_{\text{bd}}) = 0$ from $t = -T_0$ to $t = +T_0$, starting from an arbitrary density concentrated in the region $\{x \leq 0\}$ and a sufficiently large T_0 . The resulting escape probability $P_{\text{esc}}(p_0, p_2)$ is then (approximately for large T_0 and large x_{bd}) given by

$$P_{\text{esc}}(p_0, p_2) = 1 - \int_{-x_{\text{bd}}}^{x_{\text{bd}}} u(x, T_0)dx. \quad (20)$$

The result (using `chebfun` [19]) in the coordinates $q_1 = \sqrt{p_2} \in [0.1, 4]$, and $q_2 = p_0 - \sqrt{p_2} \in [-6, 4]$ is shown in Figure 3.

When one varies the noise variance D in the original system (16), keeping the original path parameters R_0 and R_2 fixed, one moves along a straight line through the origin in Figure 3. An example is shown by a red line in Figure 3. The small-noise limit is at the large- p_2 (or q_1) end, and the large noise (or slow drift) limit is at the origin.

In the coordinates $(q_1, q_2) = (\sqrt{p_2}, p_0 - \sqrt{p_2})$ the slope of all P_{esc} level curves of equal probability will approach 0 for large q_1 (or $\sqrt{p_2}$) such that the level curve for $P_{\text{esc}} = 0.5$ asymptotes to the horizontal $q_2 = p_0 - \sqrt{p_2} = 0$ as at these parameter values the deterministic system has its tipping threshold (see (6) in Section II), and the limit of large p_2 (or q_1) corresponds to the rapid drift (or small noise) limit. The q_2 coordinate of the P_{esc} level curves for $P_{\text{esc}} < 0.5$ decreases slightly faster than logarithmic in q_1 , while for $P_{\text{esc}} > 0.5$ levels the q_2 coordinate increases (slightly faster than logarithmically) for increasing q_1 .

While the numerical result is sufficient for some practical estimates, Appendix B gives approximation formulas for some regions of the (q_1, q_2) plane, which may provide additional insight into the nature of various terms.

In particular, in the parameter region below the red line $q_2 = -0.41q_1$ in Figure 3, a reasonable approximation of the escape rate at time t is provided by the leading eigenvalue γ_1 of the linear time-dependent right-hand side in the Fokker-Planck equation (19), after changing to co-moving coordinates (see Appendix B for details and Ritchie and Sieber [20] for background). This permits us to estimate escape probabilities for arbitrary parameter paths $p(t)$, after a one-off fit of the leading eigenvalue $\gamma_1(\bar{x})$ (which is a function of the current position of the deterministic trajectory $\bar{x}(t, p(t))$ in co-moving coordinates) from the deterministic trajectory $\bar{x}(t, p(t))$:

$$P_{\text{esc}}^{\text{1d}} \approx 1 - \exp \left(\int_{-\infty}^{\infty} \gamma_1(\bar{x}(t, p(t))) dt \right). \quad (21)$$

V. PROBABILITY OF TIPPING FOR THE MONSOON MODEL

We now estimate the probability of tipping for the Monsoon model by projecting the system (13,14) onto a one-dimensional output ($\mathbf{w}^T = \mathbf{w}_0^T = (-3.50, -0.99)$) and expanding it near the fold to quadratic order (in

x), and using (21). If time is measured in decades, the quadratic expansion of the monsoon model near its fold has the form $\dot{x} = p_f(A_{\text{sys}}(t) - A_{\text{sys}}^b) + x_f x^2$ where x is a dimensionless projection of the state. We add white noise of variance $2\Delta = \text{diag}(0.02, 6)$ to the monsoon model (13,14), such that

$$dx = [p_f(A_{\text{sys}}(t) - A_{\text{sys}}^b) + x_f x^2]dt + \sqrt{2D}dW_t \quad (22)$$

with $p_f = 115.30$, $x_f = 0.69$, $D = 3.04$. The paths $A_{\text{sys}}(t)$ are chosen according to equation (15)

$$A_{\text{sys}}(t) = A_{\text{sys}}^\infty + 4r\mu(1-\mu), \quad \text{and} \quad \dot{\mu} = 4\epsilon\mu(1-\mu), \quad (23)$$

where $A_{\text{sys}}^\infty = 0.47$ is the present-day value of the albedo.

Since in the probabilistic scenario, tipping is possible also for paths $A_{\text{sys}}(t)$ that do not exceed A_{sys}^b , it is useful to also consider other (especially lower) thresholds than A_{sys}^b for measuring exceedance amplitudes and times. We choose $A_{\text{sys}}^{\text{th}} = 0.5$, and, hence, consider the parameter plane $(R^{(0.5)}, t_e^{(0.5)})$, where $R^{(0.5)} = r + A_{\text{sys}}^\infty - 0.5$ is the distance of the maximal albedo along the path from a chosen albedo threshold 0.5, and $t_e^{(0.5)}$ is the corresponding exceedance time above this threshold.

Figure 4 shows the single mode approximation (21) for the solution \bar{x} of (22)–(23) for the probability of tipping $P_{\text{esc}}^{\text{1d}}$, (a fit for $\gamma_1(\bar{x})$ is given in Appendix B), on a grid of points in this $(R^{(0.5)}, t_e^{(0.5)})$ - plane. Since the mode approximation (21) is valid only in the region $q_2 < -0.41q_1$ (below the red line in Figure 3), Figure 4 leaves a part of the $(R^{(0.5)}, t_e^{(0.5)})$ -plane white. The vertical white dashed line positioned indicates the location of the deterministic fold bifurcation and the black dashed curve provides the boundary for deterministic ($D = 0$) tipping.

The results in Figure 4 show that the level curves for equal probability align with the inverse-square law for deterministic tipping only partially, namely in those parameter regions that correspond q_1 and q_2 with nearly horizontal level curves in Figure 3. For $R^{(0.5)} < 0.02$ (meaning that the fold (saddle-node) is not reached) and small $t_e^{(0.5)}$ (fast shifts) the probability of tipping is small. The probability of tipping increases if the path exceeds the fold ($R^{(0.5)} > 0.03$) or the exceedance time $t_e^{(0.5)}$ over the threshold increases. Note that the $(R^{(0.5)}, t_e^{(0.5)})$ coordinates are singular at their origin such that all equal-probability level curves pass through the origin. In Appendix B, we compare the mode approximation (21), which uses only the leading eigenvalue γ_1 of the Fokker-Planck equation for the one-dimensional projection (22), to the true probability of tipping for the full 2d system (13)–(14).

Figure 5b shows the probability of tipping for a range of times $t_e^{(0.5)}$ for which $A_{\text{sys}}(t)$ is above the threshold 0.5 for two fixed maxima $\max_t A_{\text{sys}}(t)$. Figure 5a shows example forcing paths $A_{\text{sys}}(t)$ for two different exceedance times for each fixed maximum.

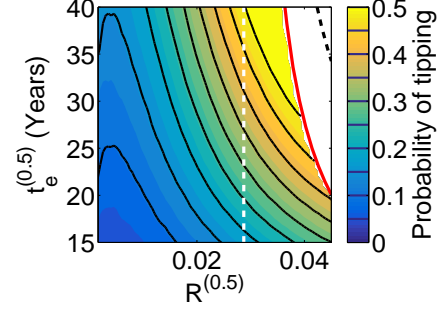


FIG. 4: Contour of the probability of tipping (21), using the leading eigenvalue γ_1 in the $(R^{(0.5)}, t_e^{(0.5)})$ - plane. Contour lines are spaced at 0.05 intervals. White dashed line indicates the fold bifurcation, black dashed curve shows the critical parameter values for deterministic tipping and the red solid curve indicates the boundary for validity of the mode approximation.

Parameters: $\mathbf{w} = (-3.50, -0.99)^T$ such that $p_f = 115.30$ and $x_f = 0.69$ in (22), $D = 3.04$.

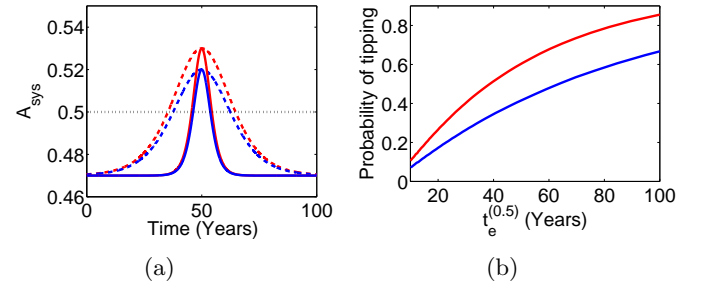


FIG. 5: Cross sections in Figure 4 for two different values of $R^{(0.5)}$: $R^{(0.5)} = 0.02$ (blue) and $R^{(0.5)} = 0.03$ (red). (a) Time profiles of planetary albedo forcing paths of a short (solid) and longer (dashed) exceedance time $t_e^{(0.5)}$ for each fixed $R^{(0.5)}$ value. Horizontal black dotted line represents the chosen threshold value $A_{\text{sys}} = 0.5$ used for the definition of $R^{(0.5)}$ and $t_e^{(0.5)}$. (b) Probability of tipping over a range of exceedance times (times for which A_{sys} is larger than 0.5).

VI. SUMMARY

In this paper, we have investigated the scenario of forcing a system over a tipping threshold (a fold of equilibria) for a short time. We provide simple criteria determining whether the forced deterministic system escapes from the family of equilibria or not. The two primary parameters of the forcing path $q(t)$ are the maximum exceedance amplitude $\max_t q(t)$ of the fold bifurcation parameter value q^b and the time t_e for which the parameter path has exceeded the fold bifurcation value. The critical curve, which separates a region of tipping and the safe region in this two-parameter plane follows an inverse-square law:

$t_e^2(\max_t q(t) - q^b) = 16/d$. The constant d can be determined from equilibria at parameters q near the critical value q^b as the ratio of the square of the decay rate to $q - q^b$.

We used a simplified version of the Indian Summer Monsoon model developed by Zickfeld [9] to demonstrate which time profiles for changing planetary albedo in the model result in (or avoid) tipping, matching the general theoretical predictions (which are only accurate if one is sufficiently close to a fold) precisely: the trade-off between exceedance amplitude and time beyond the critical value of the albedo follows the inverse-square law.

We also quantify the effect of random disturbances, modelled by white additive noise, determining a probability of tipping. For each chosen threshold q_0 near the fold we obtain level curves of equal probability in the parameter plane $(\max_t q(t) - q_0, t_e^0)$ of exceedance amplitude and exceedance time for q_0 . These level curves follow the inverse-square law in part, deviating from it (expectedly) in the large-noise (slow-drift) limit and at the origin of the $(\max_t q(t) - q_0, t_e^0)$.

ACKNOWLEDGMENTS

P.D.L.R.'s research was supported by funding from the EPSRC Grant No. EP/M008495/1, P.D.L.R has also received funding from the NERC grant No. NE/P007880/1. J.S. gratefully acknowledges the financial support of the EPSRC via Grants No. EP/N023544/1 and No. EP/N014391/1. J.S. has also received funding from the European Union's Horizon 2020 research and innovation programme under Grant Agreement No. 643073. The research materials supporting this publication can be accessed at <https://doi.org/10.6084/m9.figshare.5492914>

Appendix A: Genericity conditions on scalar output x

If equation (1), $\dot{\mathbf{y}} = f(\mathbf{y}, q)$, has a fold (saddle-node) at (\mathbf{y}^b, q^b) , then the linearization $A_1 = \partial_1 f(\mathbf{y}^b, q^b)$ is singular and has a single right nullvector \mathbf{v}_0 and a single left nullvector \mathbf{w}_0 ($A_1 \mathbf{v}_0 = 0$, $\mathbf{w}_0^T A_1 = 0$), scaled such that $\mathbf{w}_0^T \mathbf{v}_0 = 1$. If we observe the output $x = \epsilon^{-1/2} \mathbf{w}^T (\mathbf{y} - \mathbf{y}^b)$, and the projection direction $\mathbf{w} \in \mathbb{R}^n$ satisfies $\mathbf{w}^T \mathbf{v}_0 \neq 0$ (the genericity condition), we can scale the nullvector \mathbf{v}_0 such that $\mathbf{w}^T \mathbf{v}_0 = 1$. Multiplying the differential equation $\dot{\mathbf{y}} = f(\mathbf{y}, q)$ by \mathbf{w}^T , expanding f at (\mathbf{y}^b, q^b) and decomposing the state y into its scaled components via $\mathbf{y} = \mathbf{y}^b + \epsilon^{1/2} [\mathbf{v}_0 y_c + \mathbf{y}_s]$, where y_c is the scaled center direction in the fold, and \mathbf{y}_s is the scaled stable direction (defined by $\mathbf{w}_0^T \mathbf{y}_s = 0$), and considering the sped-up time $t_{\text{new}} = \epsilon^{1/2} t_{\text{old}}$ we obtain

$$\dot{x} = a_0(R_0 - R_2 t^2) + a_2 x^2 + O(\epsilon^{1/2}),$$

where

$$\begin{aligned} a_0 &= \mathbf{w}_0^T \partial_2 f(\mathbf{y}^b, q^b), \\ a_2 &= a_0 \kappa = \frac{1}{2} \mathbf{w}_0^T \partial_1^2 f(\mathbf{y}^b, q^b) \mathbf{v}_0^2, \\ R_0 &= \epsilon^{-1} (r - q^b + q^\infty), \\ R_2 &= \frac{q^\infty - q^b}{2} \Gamma''(\mu_c). \end{aligned}$$

The other genericity conditions are that the coefficients a_0 and κ are non-zero[21]. Note that the projections generating a_0 and κ involve \mathbf{w}_0 , not \mathbf{w} . Thus, the differential equation for x is (up to terms of order $\epsilon^{1/2}$) identical to the differential equation for y_c , the coordinate along the critical direction \mathbf{v}_0 . This follows from the fact that the stable direction \mathbf{y}_s is of order $\epsilon^{1/2}$, and the scaling of \mathbf{v}_0 : $x = \mathbf{w}^T (\mathbf{v}_0 y_c + O(\epsilon^{1/2})) = y_c + O(\epsilon^{1/2})$ (since $\mathbf{w}^T \mathbf{v}_0 = 1$).

For the stochastic differential equation the additive noise term, similarly, has the variance $\mathbf{w}_0^T \Delta \mathbf{w}_0$ (ignoring terms of order $\epsilon^{1/2}$).

Appendix B: Approximations of tipping probability P_{esc}

This appendix discusses different approximation methods used for calculating the tipping probability P_{esc} for various regions of the (q_1, q_2) plane.

The double exponential of $1 - P_{\text{esc}}$ satisfies a cubic fit accurately over the region shown in Figure 3:

$$1 - P_{\text{esc}} \approx \exp \left[-\exp \sum_{k=0, j \leq k}^3 c_{kj} q_1^j q_2^{k-j} \right], \quad (\text{B1})$$

where the coefficients c_{kj} are given in Appendix C, Table II. The absolute error over the region of Figure 3 is 0.024 and the cut-off relative error ($|P_{\text{esc}} - P_{\text{esc}}^{\text{approx}}| / \max(0.1, P_{\text{esc}})$) is less than 10%.

a. Slow drift approximation For small parameters p_2 (or q_1) the integration of the FPE (19) would require long time intervals (only for times of order $1/\sqrt{p_2}$ are well separated stable and unstable slow manifolds present in the deterministic part $\dot{x} = p_0 - p_2 t^2 + x^2$). However, in this regime the time-dependence of the SDE (18) is weak: the time derivative of the right-hand side $p_0 - p_2 t^2 + x^2$ is of order $\sqrt{p_2}$ for $|t| \sqrt{p_2}$ or order 1 or less. Hence, we may approximate the rate of escape at each time t using the escape rate for the static potential well corresponding to the right-hand side $p_0 - p_2 t^2 + x^2$. This escape rate is given by the dominant eigenvalue λ_0 of the linear operator on the right-hand side of the Fokker-Planck equation (19). Solving the parameter-dependent eigenvalue problem

$$-\lambda(p)u(x, p) = \partial_x^2 u(x, p) - \partial_x[(p + x^2)u(x, p)] \quad (\text{B2})$$

for its first eigenvalue λ_0 (specifically, with Dirichlet boundary conditions on the interval $[-8, 8]$ using

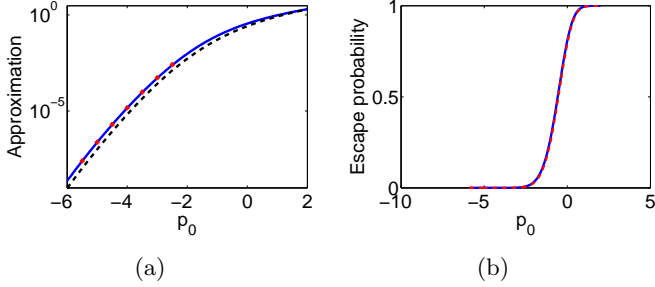


FIG. 6: Slow drift approximation: (a) shows the leading eigenvalue $\lambda_0(p)$ (blue solid) as numerically computed using (B2), the approximation given by Kramers' escape rate (red markers) and μ_0 defined in (B3). (b) compares the slow drift approximation (B3) (blue solid) to the numerical value (from Figure 3) (red dashed) at $p_2 = 0.1$. The difference always below 0.02.

`chebfun`[19]), provides the escape rate. The eigenvalue $\lambda_0(p)$ is real and positive (due to the minus sign on the left-hand side in (B2)), and exponentially small for $p \ll -1$, where the approximation with Kramers' escape rate ($\lambda_0 \approx \sqrt{-p}/\pi \exp(4p\sqrt{-p}/3)$ for the drift term in (B2) and $D = 1$) is valid. Figure 6a shows λ_0 and the Kramers' escape rate approximation. The probability of *not* escaping is then the product of all probabilities of not escaping near all times t , such that overall:

$$\begin{aligned} P_{\text{esc}} &\approx 1 - \exp\left(-2 \int_0^\infty \lambda_0(p_0 - p_2 t^2) dt\right) \\ &\approx 1 - \exp\left(-2 p_2^{-1/2} \mu_0(p_0)\right) \end{aligned} \quad (\text{B3})$$

where $\mu_0(p) = \int_0^\infty \lambda_0(p_0 - s^2) ds$ is also shown in Figure 6a. Since the eigenvalue $\lambda_0(p)$ (and its integral $\mu_0(p)$) are exponentials, approximation (B3) explains the double exponential nature of the probability P_{esc} . The logarithms of λ_0 and μ_0 fit accurately to cubic polynomials over the range shown in Figure 6 ($\mu_0(p) \approx \exp(1.35(p - 1))$) fits up to 0.02 in absolute value for $p < 0.3$; see Table II in Appendix C). Figure 6b compares the slow-drift approximation (B3) to the numerical result from Figure 3. The absolute error is always below 0.02 and the cut-off relative error ($|P_{\text{esc}} - P_{\text{esc}}^{\text{slow}}| / \max(0.1, P_{\text{esc}})$) is less than 10%. The slow drift approximation becomes more accurate for values of p_2 smaller than 0.1.

b. Single mode approximation in moving coordinates
An approach explored by Ritchie and Sieber [20] extends the slow drift approximation to a region of the parameter plane where p_2 is not small. We consider the unique solution $\bar{x}(t; p_0)$ of the deterministic ODE (dropping $\sqrt{2}dW_t$ from (18))

$$dx(t) = [p_0 - p_2 t^2 + x(t)^2] dt \quad (\text{B4})$$

satisfying $\bar{x}(t; p_0) + \sqrt{p_2}|t| \rightarrow 0$ for $t \rightarrow \infty$ (see Figure 7a). Then we make a time-dependent coordinate shift $z(t) = x(t) - \bar{x}(t; p_0, p_2)$ and consider escape of a realization of

z from the vicinity of the origin when adding stochastic disturbances to this shifted system:

$$dz = [z^2 + 2\bar{x}(t; p_0, p_2)z] dt + \sqrt{2}dW_t. \quad (\text{B5})$$

Now we apply the slow-drift approximation in the coordinate system for z (after the time-dependent shift). The eigenvalue problem for the operator on the right-hand side of the Fokker-Planck equation for (B5) is now (with Dirichlet boundary conditions)

$$-\gamma(p)u(z; p) = \partial_z^2 u(z; p) - \partial_z[(z^2 + 2p\bar{x})u(z; p)], \quad (\text{B6})$$

where the parameter p is equal to $\bar{x}(t; p_0, p_2)$. Ritchie and Sieber [20] give a way to approximate the escape rate $\gamma_1(p)$. Its numerically computed value is shown in Figure 7b (computation performed with `chebfun`[19] on the interval $[-8, 8]$). As one can see, the escape

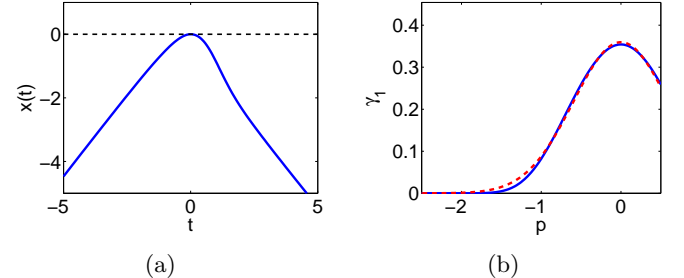


FIG. 7: (a) Trajectory of deterministic system (B4) with $p_0 = 0.59$ and $p_2 = 1$. (b) Slow drift approximation (blue solid) and numerical value (red) of escape rate $\gamma_1(p)$ for escape problem (B6).

rate $\gamma_1(p)$ has a maximum at $p = 0$. This points to a limitation of the validity for the mode approximation. When the deterministic trajectory $\bar{x}(t)$ enters the region $x > 0$, it becomes locally repelling, such that the potential $-z^3/3 - p_2 z^2$ corresponding to (B5) has a hill top at 0, but a well at $-2\bar{x}$. The region of validity for the mode approximation is thus limited to the region where $p = \bar{x} \leq 0$. This implies that the deterministic reference trajectory $\bar{x}(t; p_0, p_2)$ has to lie in $\{x \leq 0\}$ for all t . This is the case when $p_0 \leq 0.59\sqrt{p_2}$ (corresponding to the area below the red line in Figure 3).

Figure 7b also shows a fitted curve of the form $\gamma_{1,2}(\bar{x}) = \exp(-c_0 - c_2 \bar{x}^2)$ with $c_0 = 1.01$ and $c_2 = 1.41$. A 4th-order fit $\gamma_{1,4}(\bar{x}) = \exp\left(-\sum_{j=0}^4 c_j \bar{x}^{4-j}\right)$ with $c = (0.33, 0.04, 1.17, -0.01, 1.04)$ has an absolute error less than 10^{-3} and a cut-off relative error ($|\gamma_1(p) - \gamma_{1,4}(p)| / \max(0.1, \gamma_1)$) less than 10^{-2} .

Again, the probability of *not* escaping is the product of all probabilities of not escaping near all times t , such that overall

$$P_{\text{esc}} \approx 1 - \exp\left(-\int_{-\infty}^\infty \gamma_1(\bar{x}(t; p_0, p_2)) dt\right), \quad (\text{B7})$$

which equals the approximation (21) in Section IV. In contrast to the slow drift approximation (B3) the integrand γ_1 depends on the deterministic trajectory $\bar{x}(t; p_0, p_2)$. This trajectory is typically non-symmetric about $t = 0$ (see Figure 7a; in contrast to the simple parabolic path $p_0 - p_2 t^2$) such that the escape rate has to be integrated over all times. As there is no good approximation formula for the trajectory $\bar{x}(t; p_0, p_2)$ (a quadratic approximation at its maximum is typically poor), the integral has to be evaluated numerically. This evaluation can be performed in parallel to the computation of the trajectory $\bar{x}(t; p_0, p_2)$ itself. For the normal form this would be an extension of the form (assuming that the integration interval is $[-T_0, T_0]$)

$$\dot{x} = p_0 - p_2 t^2 + x^2, \quad x(-T_0) = -T_0 \quad (\text{B8})$$

$$\dot{\gamma}_{\text{acc}} = \gamma_{1,4}(x), \quad \gamma_{\text{acc}}(-T_0) = 0. \quad (\text{B9})$$

Then $P_{\text{esc}} \approx 1 - \exp(-\gamma_{\text{acc}}(T_0))$. More generally, the parameter path does not have to be parabolic: $p_0 - p_2 t^2$ may be replaced with an arbitrary function $p(t)$ satisfying $p(t) \ll -1$ for $|t| \gg 1$ (after rescaling). Moreover, x in (B9) can be the rescaled scalar output of the simulated large system (after applying scalings (4) and (17): $x(t) = \epsilon^{-1/2} D^{1/3} (a_0 \kappa)^{-1/3} w^T (y(t) - y^b)$). The initial condition for γ_{acc} should be set to 0, as (B9) evaluates the integral in (B7).

c. Accuracy of projection and approximation The projection to a one-dimensional system gives only accurate predictions for sufficiently small ϵ , that is, for sufficiently small noise and slow parameter drift. We compare the predictions from the mode approximation of the projection onto the atmospheric temperature T_a to the results of the two-dimensional monsoon model (13)–(14). To evaluate the tipping probability for the two-dimensional monsoon model we solve the Fokker-Planck equation

$$\begin{aligned} \dot{u} = & D_1 \partial_{q_a}^2 u + D_2 \partial_{T_a}^2 u - \partial_{q_a} [f_1(q_a, T_a, A_{\text{sys}}(t))u] \\ & - \partial_{T_a} [f_2(q_a, T_a, A_{\text{sys}}(t))u] \end{aligned} \quad (\text{B10})$$

on the decade timescale with noise variances $D_1 = 0.01$ and $D_2 = 3$, and Dirichlet boundary conditions on the domain $(q_a, T_a) \in [-0.04, 0.07] \times [295, 315]$ (so slightly larger than the physically realistic ranges). The paths $A_{\text{sys}}(t)$ are chosen as described in Section III (equation (15)) and Section V (equation (23)) with $A_{\text{sys}}^\infty = 0.47$ (the approximate present day value), and r and ϵ varying such that we exceed the threshold $A_{\text{sys}} = 0.5$ by time $t_e^{(0.5)} \in [15, 40]$ years and amplitude $R^{(0.5)} \in [0, 0.045]$. For each simulation, we start from the eigenvector for the dominant (close to 1) eigenvalue of the Fokker-Planck operator on the right-hand side of (B10). The total simulation time period is chosen such that, after the transient time period, A_{sys} starts from close to its current day value, namely 0.471, and returns back to this value again at the end of the total simulation period. The escape

probability is then calculated as

$$P_{\text{esc}}^{2d} = 1 - \int_{q_a, T_a} u(q_a, T_a, t_{\text{end}}) dq_a dT_a, \quad (\text{B11})$$

at the end of an overall integration period (neglecting the escape during the transient time period). The resulting escape probabilities are shown in Figure 8a. The

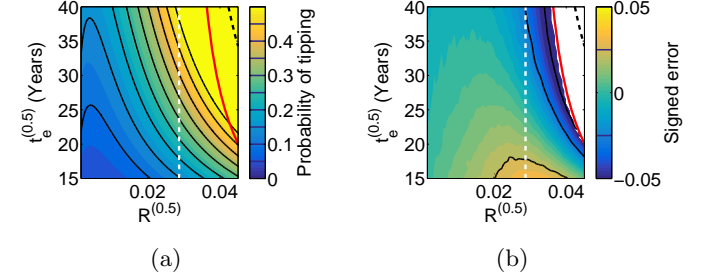


FIG. 8: Comparison between the escape probability as computed from the full two-dimensional model to its projection and approximation (21). (a) Escape probability P_{esc}^{2d} , as computed using (B10) and (B11). (b) Probability error of the mode approximation depicted in Figure 4 calculated as $P_{\text{esc}}^{1d} - P_{\text{esc}}^{2d}$. As in Figure 4, white dashed lines indicates the fold bifurcation, black dashed curve the critical parameter values for deterministic tipping and the red solid curve indicates the boundary for validity of the mode approximation.

one-dimensional projection of the monsoon model (5) is extracted from the observable temperature T , using a second-order approximation of the known equilibrium curve $(q_a, T_a, A_{\text{sys}})$ and the attraction rate toward stable equilibria nearby. In practice, these quantities may have to be estimated from observations or model outputs. Then we use a modification of (B8), replacing the parabolic parameter path with the (rescaled) forcing of the planetary albedo (23):

$$\dot{x} = D^{-2/3} a_0^2 \kappa (A_{\text{sys}}(D^{-1/3} t) - A_{\text{sys}}^b) + x^2. \quad (\text{B12})$$

In (B12) $A_{\text{sys}}(t)$ is given by (23), $D = \mathbf{w}_0^T \text{diag}(0.01, 3) \mathbf{w}_0 = 3.04$ with $\mathbf{w}_0 = (-3.50, -0.99)^T$, $A_{\text{sys}}^b \approx 0.5287$, $\kappa \approx 6 \cdot 10^{-3}$ and $a_0 \approx 115.30$ ($a_0^2 \kappa$ was estimated from decay rate and equilibrium curve of the 2d monsoon model).

The difference between the true escape rate and the mode approximation for the one-dimensional projected system (shown in Figure 8b) is less than 0.05 in absolute value everywhere in the region. The main source of error is that, due to the large noise variance, the system visits parts of the phase space where the quadratic approximation to the fold and the projection onto a single dimension are not accurate (the time scale separation between the two dimensions is only large close to the fold).

Appendix C: Monsoon parameter values and fitting coefficients

One of the aims of Section III was to provide a simplification to the Indian Summer Monsoon model used by Zickfeld [9], though retaining the key dynamics behind the mechanisms of the monsoon. Table I lists all the parameters and their values used in the simplified monsoon model. The values of the fitting coefficients for the approximations of tipping probability P_{esc} are listed in Table II.

TABLE I: Table of parameters used in Indian Summer Monsoon model

Parameter	Value	Unit
T_{oc}	300	K
T_0	273.2	K
q_{oc}	0.0190	1
q_{sat}	0.0401	1
\mathcal{L}	2.5×10^6	$m^2 s^{-2}$
C_E	3.4375×10^{-4}	$mm s^{-1} K^{-1}$
C_P	0.0027	$mm s^{-1}$
C_{mo}	6.9021×10^{-4}	$mm s^{-1} K^{-1}$
C_{ml}	1.6213×10^{-4}	$mm s^{-1} K^{-1}$
C_{L1}	1.6642	$Kg s^{-3} K^{-1}$
C_{L2}	-263.3753	$Kg s^{-3}$
$F_{\downarrow}^{SL,TA}$	443.6250	$Kg s^{-3}$
C_H	0.7136	$Kg s^{-3} K^{-2}$
θ_{oc}	300.2356	K
Γ_0	0.0053	$K m^{-1}$
Γ_1	5.5×10^{-5}	m^{-1}
Γ_2	1000	1
Γ_a	0.0098	$K m^{-1}$
z_h	5.1564×10^3	m
I_q	2.0636×10^3	mm
I_T	1.1958×10^9	$Kg s^{-2} K^{-1}$
β	3.1710×10^{-9}	decades s^{-1}

[1] T. M. Lenton, H. Held, E. Kriegler, J. W. Hall, W. Lucht, S. Rahmstorf, and H. J. Schellnhuber, *Proceedings of the National Academy of Sciences* **105**, 1786 (2008).

[2] H. Held and T. Kleinen, *Geophysical Research Letters* **31** (2004).

[3] M. M. Holland, C. M. Bitz, and B. Tremblay, *Geophysical Research Letters* **33** (2006).

[4] C. A. Boulton, L. C. Allison, and T. M. Lenton, *Nature Communications* **5** (2014).

[5] W. F. Laurance, B. Dell, S. M. Turton, M. J. Lawes, L. B. Hutley, H. McCallum, P. Dale, M. Bird, G. Hardy, G. Prideaux, *et al.*, *Biological Conservation* **144**, 1472 (2011).

[6] G. F. Clark, J. S. Stark, E. L. Johnston, J. W. Runcie, P. M. Goldsworthy, B. Raymond, and M. J. Riddle, *Global Change Biology* **19**, 3749 (2013).

[7] W. Yan, R. Woodard, and D. Sornette, *Physics Procedia* **3**, 1641 (2010).

[8] P. Ashwin, C. Perryman, and S. Wieczorek, *Nonlinearity* **30**, 2185 (2017).

TABLE II: Table of fitting coefficients

Expression	coefficient	Value
Eq. (B1)	c_0	0.98
	c_1	(1.41, -0.97)
	c_2	(-0.22, -0.28, 0.33)
	c_3	(0.01, 0.03, 0.04, -0.04)
$\log \lambda_0(s) = \sum_{k=0}^3 c_k s^k$ in Eq. (B3)	c	(-1.3433, 1.3659, -0.2347, 0.0277)
$\log \gamma_{1,4}(\bar{x}) = \sum_{k=0}^4 c_k \bar{x}^k$ in Eq. (B9)	c	(-1.0388, 0.0058, -1.1687, -0.0409, -0.3326)

[9] K. Zickfeld, *Modeling large-scale singular climate events for integrated assessment*, Ph.D. thesis, Universitätsbibliothek (2004).

[10] A. Levermann, J. Schewe, V. Petoukhov, and H. Held, Proceedings of the National Academy of Sciences **106**, 20572 (2009).

[11] K. Zickfeld, B. Knopf, V. Petoukhov, and H. Schellnhuber, Geophysical Research Letters **32** (2005).

[12] P. D. Ditlevsen and S. J. Johnsen, Geophysical Research Letters **37** (2010).

[13] M. Scheffer, J. Bascompte, W. A. Brock, V. Brovkin, S. R. Carpenter, V. Dakos, H. Held, E. H. Van Nes, M. Rietkerk, and G. Sugihara, Nature **461**, 53 (2009).

[14] V. Dakos, M. Scheffer, E. H. van Nes, V. Brovkin, V. Petoukhov, and H. Held, Proceedings of the National Academy of Sciences **105**, 14308 (2008).

[15] T. M. Lenton, Nature Climate Change **1**, 201 (2011).

[16] M. Scheffer, S. R. Carpenter, T. M. Lenton, J. Bascompte, W. Brock, V. Dakos, J. Van De Koppel, I. A. Van De Leemput, S. A. Levin, E. H. Van Nes, *et al.*, science **338**, 344 (2012).

[17] P. Ritchie and J. Sieber, Chaos **26**, 093116 (2016).

[18] T. Lenton, V. Livina, V. Dakos, E. Van Nes, and M. Scheffer, Philosophical Transactions of the Royal Society of London A: Mathematical, Physical and Engineering Sciences **370**, 1185 (2012).

[19] T. A. Driscoll, N. Hale, and L. N. Trefethen, *Chebfun guide* (Pafnuty Publications, Oxford, <http://www.chebfun.org/>, 2014).

[20] P. Ritchie and J. Sieber, Phys. Rev. E **95**, 052209 (2017).

[21] Y. A. Kuznetsov, *Elements of Applied Bifurcation Theory*, 3rd ed., Applied Mathematical Sciences, Vol. 112 (Springer-Verlag, New York, 2004) pp. xxii+631.